Imaging of a Vortex Lattice Transition in YNi_2B_2C by Scanning Tunneling Spectroscopy

Hideaki Sakata, Morimi Oosawa, Ken Matsuba, and Nobuhiko Nishida
Tokyo Institute of Technology, 2-12-1 Ookayama, Meguro-ku, Tokyo 152, Japan

Hiroyuki Takeya and Kazuto Hirata
National Research Institute for Metals, 1-2-1 Sengen, Tsukuba, Ibaraki 305, Japan
(Received 19 July 1999)

The vortex lattices in YNi_2B_2C under the magnetic fields H up to 3 T applied along both the a and the c axes have been studied by scanning tunneling spectroscopy at 4.2 K. The vortex lattice transition has been found to occur in different manners for $H \parallel a$ and $H \parallel c$; in $H \parallel a$ a slightly distorted hexagonal vortex lattice has been found to transform to a nearly square one above 1.0 T with increasing H, while in $H \parallel c$ the transition occurs at a much lower field around 0.1 T. The unconventional steep increase of the quasiparticle density of states outside the vortex core has also been found well below H_{c2}.

PACS numbers: 74.50.+r, 74.60.Ec, 74.60.Ge

The family of quaternary intermetallic compounds, RNi_2B_2C, where R denotes rare-earth elements, presents a rich variety of interesting physical properties [1]. Coexistence of superconductivity and antiferromagnetic ordering has been reported in Dy, Ho, and Er compounds [2]. Y and Lu compounds exhibit superconductivity with a rather high superconducting transition temperature about 15 K [1]. These compounds have been studied intensively as typical superconductors in borocarbides. The structure and dynamics of the vortex lattice in these materials have also attracted much attentions from those who work on vortices in superconductors. A vortex lattice is square in the external magnetic field, H, higher than 0.1 T applied parallel to the c axis of the tetragonal crystal [3–5]. The vortex lattice undergoes a square-to-hexagonal transition around 0.1 T with decreasing magnetic fields in YNi_2B_2C [5]. The transition has been described in terms of the Ginzburg-Landau theory and the London model with nonlocal extension considering the anisotropy in the ab plane of the underlying crystal [3,6]. These models have succeeded in explaining the square-to-hexagonal transition in borocarbides qualitatively for $H \parallel c$. The theories have predicted that the vortex lattice undergoes the transition at a much higher magnetic field for $H \parallel a$ than that for $H \parallel c$ owing to the anisotropy in the ac plane [6]. The investigation of the vortex lattice transition in the magnetic field applied along the a axis will be a good test of the validity of these models.

In order to observe the vortex lattice in YNi_2B_2C, we performed the scanning tunneling microscopy (STM) and scanning tunneling spectroscopy (STS) measurements. STM/STS is able to measure the quasiparticle density of states, $N_s(E, r)$, where E is the energy of quasiparticles and r is a position of the STM tip on the surface. Thus, the vortex lattice can be imaged even at high magnetic fields where the spacing between vortices is smaller than the penetration depth λ. Owing to the difficulty of surface preparation, however, an image of the vortex lattice has been observed in only several materials by STS: a cleaved surface of 2H-$NbSe_2$ [7] and $Bi_2Sr_2CaCu_2O_8$ [8], an as grown surface of $YBa_2Cu_3O_7$ which was grown in a special crucible [9], and a chemically etched surface of $LuNi_2B_2C$ [3]. In our previous STS experiments on $CeRu_2$ whose surface is easily oxidized or contaminated in air, we succeeded in a vacuum tunneling spectroscopy and in measuring the one-particle density of states of quasiparticles by cracking a single crystal in vacuum at liquid helium temperature [10]. We applied this surface preparation of cracking to YNi_2B_2C. The STS images of the vortex lattice in YNi_2B_2C have been observed on the cracked surface for the first time. The vortex lattices have been imaged through measurements of $N_s(E, r)$, and the vortex lattice transitions have been observed in the external magnetic fields up to 3 T applied parallel to both the a and the c axes. We have also observed the unconventional steep increase in $N_s(E = 0, r)$ outside the vortex core with increasing magnetic fields even well below H_{c2}.

A single crystal of YNi_2B_2C was grown by the floating zone method. The crystallographic axes of the crystal were determined by the x-ray diffraction technique and the sample was cut out from the single crystal with an accuracy within 2°. A typical size of the sample is $2.0 \times 1.0 \times 1.0$ mm^3. From dc magnetization measurements, T_c was determined to be 14.0 K and H_{c2} parallel to the a and the c axes at 4.2 K were 7 and 6 T, respectively. The STM/STS measurements were performed with our homemade low temperature scanning tunneling microscope (LT-STM) which is able to be operated in vacuum down to 2.2 K in magnetic fields up to 14.5 T. In order to obtain a clean surface, we pushed a single crystal sample against an edge of the thin blade and cut or cracked the sample at the sample holder of the microscope at 4.2 K prior to STS or STM measurements. With this method, we prepared the clean ab and ac surfaces. A mechanically sharpened Pt-Ir tip was used for STS and STM measurements. External magnetic fields from 0.1 up to 3.0 T were applied along the a or the c axis, that is, parallel to

the tip-sample direction. The misorientation between the crystallographic axes and the magnetic field is within 2°. Thus the influence of a field misorientation is negligible. In all measurements, external magnetic fields were applied to the sample above T_c before cooling the sample down to 4.2 K. The details of the scanning tunneling microscope will be published elsewhere.

The shapes of tunneling spectra measured on the cracked surface in zero magnetic field were independent of the tip-sample separation and reproducible over the surface, which confirms true vacuum tunneling. The superconducting energy gap was estimated by fitting the experimental curve to the BCS expression of a density of states of quasiparticles with a broadening parameter Γ [11]. Typical fitting parameters were Δ of 1.8 meV and Γ of 0.13 meV on the ab surface at 4.2 K in zero magnetic field; $2\Delta/k_B T_c = 3.3$. Our result is in agreement with the results of STM and break junction experiments showing weak-coupling superconductivity [3,12].

The STM topographs of the cracked ab and ac surfaces are shown in Figs. 1(a) and 1(b), respectively. The ab surface is flat with the roughness less than 1 nm, but an atomic image has not been observed. A step with a few unit cell height can be seen at the upper left of Fig. 1(a). The flat surfaces will reflect the layer structure of YNi_2B_2C, though YNi_2B_2C does not have a plane of cleavage. The cracked ac surface exhibits protrusions of 15 nm in height and a few tens nm in size and each protrusion has microstructures as shown in the inset of Fig. 1(b); the average size of the microstructure is about 2 nm in height and diameter. Almost the same microstructure has been observed on the cracked surface of $CeRu_2$ [10]. It is likely that the cracking of the sample at low temperature might have caused these microstructures on the surface. The cracked ac surface was not parallel to the ac plane and it made a tilt angle of about 30° which is obtained from the STM image. In Fig. 1(b), a uniform tilt of the surface was subtracted from the original STM image.

The spatial dependence of I-V characteristics has been measured at 128 × 128 or 64 × 64 points on the cracked YNi_2B_2C surfaces. The differential tunneling conductances, which are proportional to $N_s(E, r)$, have been obtained by differentiating the I-V curves numerically. In the magnetic field of 0.5 T applied parallel to the c axis, the spatial variation of $N_s(E = 0, r)$ at 4.2 K is shown in Fig. 1(c). $N_s(E = 0, r)$ at each point were normalized with the value at 10 meV which is much larger than the energy gap of 1.8 meV. A square vortex lattice has been clearly observed, where the vortex cores are imaged as an increase of $N_s(E = 0, r)$, seen as white regions. The diagonals of the square unit cell are parallel to the a axis of the crystal lattice, which is consistent with the results of the small angle neutron scattering experiments [4,5].

In contrast to the square vortex lattice observed for $H \parallel c$, a slightly distorted triangular vortex lattice was observed at 0.45 T for $H \parallel a$ as shown in Fig. 1(d). The vortex lattice image in Fig. 1(d) was taken at the same place where Fig. 1(b) was observed; STS is efficient to observe vortices in spite of the surface roughness about 15 nm. The diagonals of the oblique unit cell of the vortex lattice are parallel to the a and the c axes of the crystal lattice, indicating that the anisotropy of the underlying crystal affects the shape of the vortex lattice.

Figure 2 shows dI/dV spectra measured at the center of a vortex core and a middle point of nearest neighbor

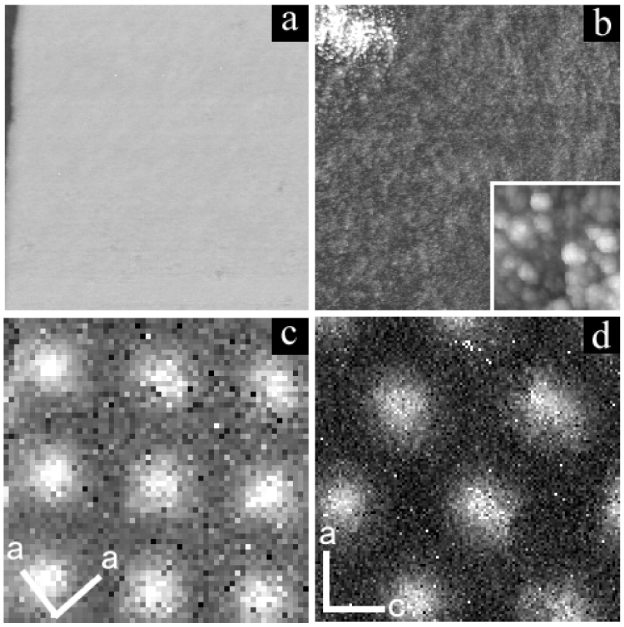

FIG. 1. 180 nm × 180 nm STM image of (a) the ab surface and (b) the ac surface. The inset is a magnified image of 10 nm × 10 nm. 180 nm × 180 nm $N_s(E = 0, r)$ map (c) under 0.5 T for $H \parallel c$ and (d) under 0.45 T for $H \parallel a$. (a) and (c), (b) and (d) are observed at the same place.

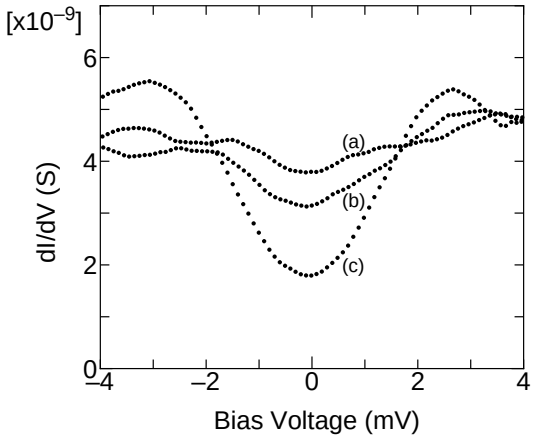

FIG. 2. The observed dI/dV spectra on the ab surface at 4.2 K under 0.5 T (a) at the center of a vortex core, (b) at 9 nm apart from the center, and (c) at a middle point of nearest neighbor vortices.

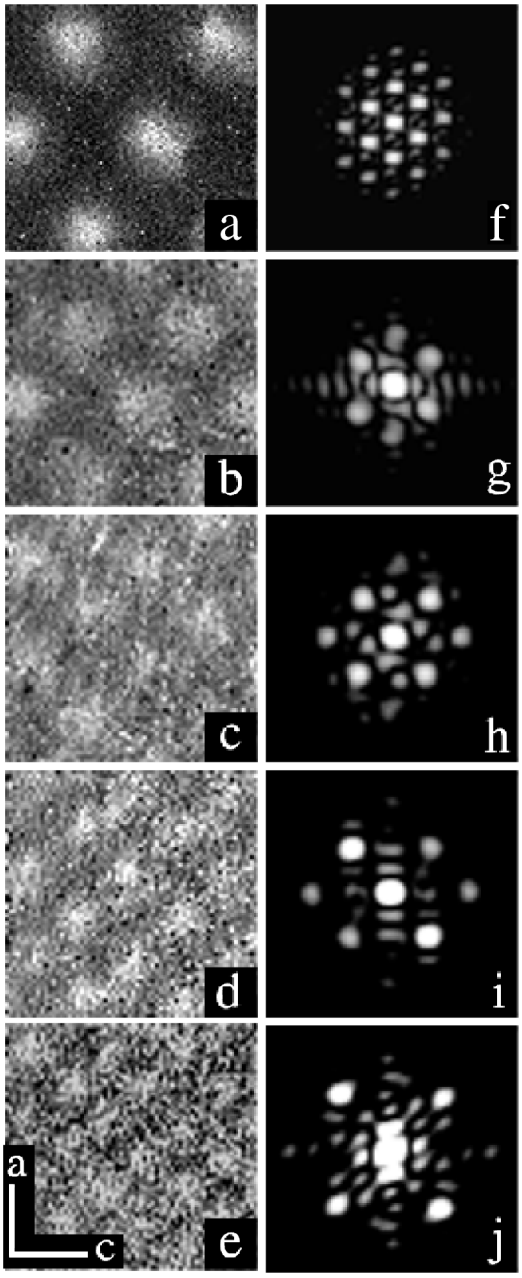

FIG. 3. A series of $N_s(E = 0, r)$ map for $H \parallel a$ at 4.2 K under (a) 0.45 T, (b) 0.75 T, (c) 1.0 T, (d) 1.5 T, and (e) 2.5 T (150 nm $\times$ 150 nm). (f)–(j) Fourier transformed images of (a)–(e).

vortices on the ab surface. The spectrum at the center of the core shows the increase of the differential conductance around 0 meV and the reduction around ± 3 meV in comparison with the spectrum outside the core. We did not detect the bound state of quasiparticles in a vortex core on both the ab and the ac surfaces as observed in 2H-$NbSe_2$ [7]. From the residual resistivity ratio, the mean free path of the sample is estimated to be about 4 nm which is shorter than a vortex core diameter. This may bring about the disappearance of the bound state of quasiparticles in a vortex core [13].

We have studied how the configuration of the vortices will change with changing applied magnetic fields in the field cooling condition. In $H \parallel c$, when it is reduced to 0.1 T, the square vortex lattice observed in 0.5 T has changed to a triangular lattice. This result indicates the vortex lattice transition occurs around 0.1 T for $H \parallel c$. Through the transition, the diagonals of the oblique unit cell are parallel to the a axis. In the magnetic field along the a axis, when it is increased from 0.45 to 3.0 T, a slightly disordered triangular lattice at 0.45 T transforms continuously into a nearly square lattice around 1.0 T. The STS images of the vortex lattices in the $H \parallel a$ axis are shown in Fig. 3 as well as their 2D Fourier transforms. Above 1.0 T, the apex angle of the oblique unit cell was constant. The diagonals of the oblique unit cell are along the a or the c axis, irrespective of the magnitude of the applied magnetic field. In order to obtain the apex angle β of the oblique unit cell of the vortex lattice, we performed Fourier transformations of the vortex lattice images. The apex angle β_a opening toward the a direction and β_c opening toward the c direction are plotted in Fig. 4. With increasing magnetic fields, β_a and β_c approach continuously toward 85° and 95°. Above 1.0 T, they keep constant values. The vortex lattice transition occurs near 1.0 T for $H \parallel a$. This makes quite a contrast to the case for $H \parallel c$ where the transition occurs at a much lower field around 0.1 T. The longer diagonal of the rhombus takes the direction parallel to either the a or the c axis as seen in Fig. 4. This may indicate the existence of two domains equivalent to each other with respect to the rotation of 90°. Looking into the results of Fig. 4 more in detail, we notice that the direction of the rhombus may depend on the magnitude of the applied magnetic field. If this is true, the longer diagonal of the rhombus is parallel to the a axis below 0.75 T and to the c axis above 0.85 T. To confirm this we need further investigation. The averaged β_c above 1.5 T was 85°. This deviation of β from 90° reflects the anisotropy in the ac plane.

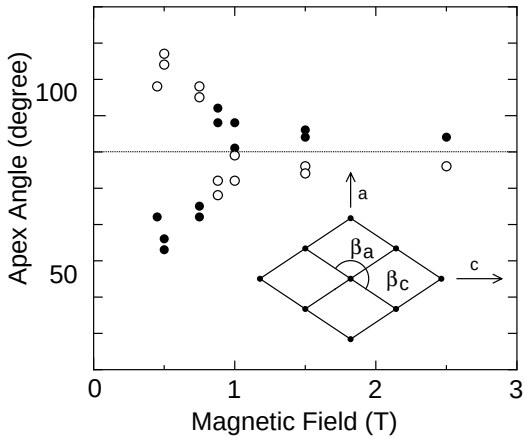

FIG. 4. Apex angle β_a opening toward the a direction (closed circle) and β_c opening toward the c direction (open circle) as a function of magnetic field applied along the a axis.

In order to explain the vortex lattice transition in borocarbides, Kogan *et al.* have used nonlocal corrections to the London model and calculated stable configurations of the vortices as a function of an applied magnetic field [6]. The model has predicted that in the case of $H \parallel c$, a stable square vortex lattice at high magnetic fields transforms into a distorted triangular lattice at H_2 in the notation of Kogan *et al.* and β decreases towards 60° as the applied magnetic field is decreased. From our present STS experiments, in high magnetic fields of $H \parallel a$, the stable configuration has been found to be a slightly distorted square lattice with β of 85° and H_2 was determined to be 1 T which is higher than in $H \parallel c$. The higher H_2 of YNi_2B_2C for $H \parallel a$ has been explained by the London model as follows [6]: As an effective range of the nonlocal effect is the order of a superconducting coherence length, ξ_o. In superconductors with a smaller ξ_o the transition is expected to occur at the shorter intervortex distance, that is, at the higher applied magnetic field. YNi_2B_2C or $LuNi_2B_2C$ is anisotropic and the magnitude of the second critical magnetic fields H_{c2} is ordered as $H_c > H_{ab} > H_a$ against crystal axis orientations. This means $\xi_c < \xi_{ab}$. Therefore, in these materials, as the effective range of the nonlocal effect shrinks for $H \parallel a$, the transition moves to a higher magnetic field in the case of $H \parallel a$ and the observed H_2 of 1 T is higher than 0.1 T for $H \parallel c$.

We also observed that the vortex lattices got disordered above 2 T. When the vortex lattice images were taken at several areas at 2 T, a few images among them have shown irregular configurations of vortices; the positions of vortices deviate from the lattice points. Furthermore, it was difficult to observe the regular vortex lattice in the magnetic field of 3 T. Considering that all the vortex lattices observed below 1.5 T were regular, we can conclude that the disorder in the vortex lattice increases with increasing magnetic fields above 2 T. The small angle neutron scattering experiments have observed similar things [4,5]. The disorder of the vortex lattice appears to depend on the quality of the samples. The precise experiments are now in progress.

In YNi_2B_2C we have found the steep increase in $N_s(E = 0, r_m)$, where r_m is a middle point of nearest neighbor vortices, with increasing the magnetic fields as shown in Fig. 5. The increase in $N_s(E = 0, r_m)$ in YNi_2B_2C is much steeper than that of 2H-$NbSe_2$ [14], which is thought to be an ordinary BCS superconductor. At half of H_{c2}, there is almost no difference between $N_s(E = 0, r_m)$ and $N_s(E = 10\ \mathrm{meV}, r_m)$ which is observed outside the energy gap. This makes observations of the vortex lattice in YNi_2B_2C above 3 T very difficult. This may have relation with the observation of the de Haas–van Alphen effect of YNi_2B_2C far below H_{c2} [15]. The increase in $N_s(E = 0, r_m)$ observed in this study can account for the deviation from the H linear dependence of the coefficient of the T linear term, $\gamma(H)$,

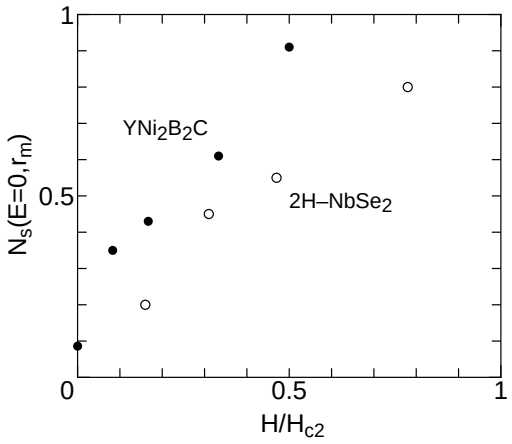

FIG. 5. Magnetic field dependence of $N_s(E = 0, r_m)$, where r_m is a middle point of nearest neighbor vortices, in YNi_2B_2C (closed circle) and in 2H-$NbSe_2$ (open circle). $N_s(E = 0, r_m)$ are normalized with $N_s(E = 10\ \mathrm{meV}, r_m)$. Magnetic field is applied along the c axis and normalized with H_{c2} of 6 T for YNi_2B_2C and 3.2 T for 2H-$NbSe_2$.

in specific heat in $LuNi_2B_2C$ [16]. Although Nohara *et al.* ascribed the deviation of $\gamma(H)$ to d-wave symmetry of the Cooper pairing [16], the anisotropic increase in $N_s(E = 0, r)$ around the vortices has not been observed as seen in Figs. 1(c) and 1(d). Therefore, YNi_2B_2C is concluded to be a conventional BCS superconductor. The understanding of the reason why the low energy quasiparticle excitations are induced by magnetic fields more in YNi_2B_2C than in other conventional superconductors needs further investigations.

This work is in part supported by a Grant-in-Aid for CREST of the Japanese Science and Technology Corporation, a Grant-in-Aid for creative basic research in "Surface and Interface," and a Grant-in-Aid for scientific research of the Ministry of Education, Science and Culture.

[1] R. J. Cava *et al.,* Nature (London) **20**, 252 (1994); R. Nagarajan *et al.,* Phys. Rev. Lett. **72**, 274 (1994).
[2] B. K. Cho *et al.,* Phys. Rev. B **52**, R3844 (1995).
[3] Y. De Wilde *et al.,* Phys. Rev. Lett. **78**, 4273 (1997).
[4] M. R. Eskildsen *et al.,* Phys. Rev. Lett. **79**, 487 (1997).
[5] M. Yethiraj *et al.,* Phys. Rev. Lett. **78**, 4849 (1997).
[6] V. G. Kogan *et al.,* Phys. Rev. B **55**, R8693 (1997).
[7] H. F. Hess *et al.,* Phys. Rev. Lett. **62**, 214 (1989).
[8] Ch. Renner *et al.,* Phys. Rev. Lett. **80**, 3606 (1998).
[9] I. Maggio-Aprile *et al.,* Phys. Rev. Lett. **75**, 2754 (1995).
[10] H. Sakata *et al. (*to be published).
[11] R. C. Dynes *et al.,* Phys. Rev. Lett. **41**, 1509 (1978).
[12] T. Ekino *et al.,* Phys. Rev. B **53**, 5640 (1996).
[13] U. Klein, Phys. Rev. B **41**, 4819 (1990).
[14] S. Kaneko *et al.,* Czech. J. Phys. **46**, Suppl. S2, 887 (1996).
[15] T. Terashima *et al.,* Phys. Rev. B **56**, 5120 (1997).
[16] M. Nohara *et al.,* J. Phys. Soc. Jpn. **66**, 1888 (1997).